


RESEARCH ARTICLE

MALDI MS Imaging at Acquisition Rates Exceeding 100 Pixels per Second

Antonín Bednařík,^{1,2} Markéta Machálková,¹ Eugene Moskovets,³ Kateřina Coufalíková,¹ Pavel Krásenský,¹ Pavel Houška,⁴ Jiří Kroupa,⁴ Jarmila Navrátilová,^{5,6} Jan Šmarda,⁵ Jan Preisler^{1,2} 

¹Department of Chemistry, Faculty of Science, Masaryk University, Kamenice 5, 625 00, Brno, Czech Republic

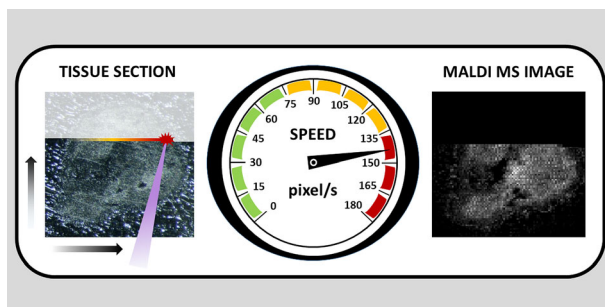
²Central European Institute of Technology (CEITEC), Masaryk University, Brno, Czech Republic

³MassTech Inc., Columbia, MD, USA

⁴Faculty of Mechanical Engineering, Brno University of Technology, Brno, Czech Republic

⁵Department of Experimental Biology, Faculty of Science, Masaryk University, Brno, Czech Republic

⁶Center for Biological and Cellular Engineering, International Clinical Research Center, St. Anne's University Hospital, Brno, Czech Republic



Abstract. The practicality of matrix-assisted laser desorption/ionization (MALDI) time-of-flight (TOF) mass spectrometry (MS) applied to molecular imaging of biological tissues is limited by the analysis speed. Typically, a relatively low speed of stop-and-go micromotion of XY stages is considered as a factor substantially reducing the rate with which fresh sample material can be supplied to the laser spot. The sample scan rate in our laboratory-built high-throughput imaging TOF

mass spectrometer was significantly improved through the use of a galvanometer-based optical scanner performing fast laser spot repositioning on a target plate. The optical system incorporated into the ion source of our MALDI TOF mass spectrometer allowed focusing the laser beam via a modified grid into a 10- μm round spot. This permitted the acquisition of high-resolution MS images with a well-defined pixel size at acquisition rates exceeding 100 pixel/s. The influence of selected parameters on the total MS imaging time is discussed. The new scanning technique was employed to display the distribution of an antitumor agent in 3D colorectal adenocarcinoma cell aggregates; a single MS image comprising 100 \times 100 pixels with 10- μm lateral resolution was recorded in approximately 70 s.

Keywords: Mass spectrometry imaging, Laser beam scanning, MALDI, TOF, MSI, High throughput, Grid ion source, 3D cell aggregates, Spheroids, Colorectal adenocarcinoma

Received: 13 May 2018/Revised: 10 September 2018/Accepted: 4 October 2018/Published Online: 19 November 2018

Introduction

Matrix-assisted laser desorption/ionization (MALDI) mass spectrometry imaging (MSI) is becoming a widely

accepted method for multiplex label-free molecular mapping of biological tissues. In the past few years, major efforts have been made to improve every aspect of the method. This led to the development of more reproducible sample preparation [1–5] techniques allowing micrometer range lateral resolution [6–8]. Also, more advanced MS systems with high throughput [9–12], high sensitivity, resolving power [13, 14], and novel designs of MALDI sources [8, 15, 16] were developed. Postionization of the MALDI plume using an additional and more powerful laser (MALDI-2) was introduced to

Electronic supplementary material The online version of this article (<https://doi.org/10.1007/s13361-018-2078-8>) contains supplementary material, which is available to authorized users.

Correspondence to: Jan Preisler; e-mail: preisler@chemi.muni.cz

dramatically boost the ion yields in MSI analyses [17, 18]. Attention was also paid to improve data handling and the processing rate of huge datasets generated by MSI [19]. The imzML format was established as a standard for MSI data [20]. Sophisticated software tools to manage and interpret data sets have been developed [21]. It is believed that the technological paradigm shift, which MALDI MSI represents, will play an essential role in such important areas as molecular pathology and biomarker discovery in the years to come [22].

MALDI, with its pulsed character of ion generation, combines naturally with axial time-of-flight (TOF) analyzers. In the ion source of the TOF MS system, the ions are first formed after each laser pulse and, after some delay, are accelerated in the ion extraction region. The TOF analyzer provides a much higher rate of spectral acquisition compared to the quadrupole traps and Fourier transform analyzers. Using acceleration voltages exceeding 15 kV, mass spectra representing a 100–10,000 m/z range can be recorded with intervals of a few hundred microseconds. Modern high-resolution axial TOF MS instruments can provide high spectral quality (high signal-to-noise ratios, high resolving power, and sub ppm mass accuracy). A tremendous throughput potential of TOF mass spectrometers commanded incorporation of solid-state lasers with repetition rates of up to 10 kHz [23, 24], which have been becoming the standard in recent MALDI TOF mass spectrometers. In TOF MS analysis, typically tens or hundreds of single pulse spectra have to be accumulated in order to enhance signal-to-noise ratio. Obtaining high spectral quality data at a rate of up to 50 averaged spectra per second has been demonstrated [11]. In general, the sample throughput demonstrated by the MALDI TOF systems is limited by the efficiency of sample utilization; the sample throughput drops with increasing number of laser shots per spot. Due to the necessity to process vast arrays of generated data, an important limitation is also a rather slow software processing speed.

In the case of MALDI TOF MS imaging operated in the laser microprobe arrangement [25], the throughput strongly depends on a sampling mode. In the traditional sampling mode, characterized by step translations of the XY stages with fixed position of the laser beam during signal acquisition, the MS image acquisition time is very long, especially for the cases when 100×100 pixels or larger images with high lateral resolution are generated. Due to the relatively slow mechanical response of the motorized XY stages, a large fraction of the imaging time is wasted by waiting for the target plate to be settled after the completion of each translation step. The TOF analyzer is heavily under used in this mode, especially when utilizing kHz lasers. In this case, the effective analysis time (i.e., the time the ions travel in the TOF MS analyzer) constitutes just a few percent of the total time (i.e., the time spent for the entire imaging experiment). The exact efficiency depends on the TOF MS instrument configuration (i.e., flight tube length, applied voltages, etc.), number of shots fired per pixel, pixel-to-pixel distance, the rate of data acquisition and agility of motorized sample translation system. The target step-by-step translation mode is outperformed by the continuous raster sampling mode; in the latter, the target moves at a constant speed with the laser

continuously firing. The continuous raster sampling can boost the throughput by the factor of 5 to 10 at a cost of more complicated definition of the true pixel size [9, 11]. Also, MALDI TOF MS instruments operating as an ion microscope (i.e., exploiting wide desorption laser spot, stigmatic ion optics, and pixelated ion detector) have a great potential to provide rapid imaging of large areas with high spatial resolution [26–28]. A fast galvanometer-based optical scanner, previously used for multiplex analysis of deposited streaks from capillary electrophoresis in MALDI TOF MS [23], was adapted for scanning mode MSI. This mode featured laser rastering in well-defined steps over the stationary sample with step translations of the target in another direction to achieve high acquisition rates while maintaining discrete pixels [29, 30]. An acquisition rate of about 17 pixel/s (4-kHz laser, 100 shots per pixel, 100,000 data points) was demonstrated using laser beam scanning. Using this mode, the imaging time was decreased by almost an order of magnitude in comparison to a step scan (raster) mode utilized in commercial TOF MS instruments. The main shortcoming of our original design was a limited lateral resolution along the axis of laser scans due to the formation of elliptically shaped laser spots on the sample. The elliptically shaped spot stemmed from the necessity for the laser beam to bypass the extraction grid under an unfavorable (obtuse) angle of incidence. It is also necessary to note that more recently, a commercial TOF analyzer with two optical scanners redirecting the laser beam under the continuously moving target was introduced to increase the MSI throughput [12, 31].

In this paper, we demonstrate the operation of an axial TOF MS system with modified planar grid electrodes. Modification of both the ion source and laser optics of our laboratory-built MS system was aimed at enhancing MSI performance in terms of both speed and lateral resolution. A 1.5-mm \times 0.5-mm rectangular window was created in the fine-mesh metal grid covering the hole in the ion extraction electrode of the MALDI ion source to facilitate scanning of the laser beam directly through the grid in a horizontal direction. The laser beam was aimed at the target almost orthogonally without being blocked by the grid wires during the scans. A lens with a short focal length was mounted closer to the target plate to allow fine laser focusing. Combining the step motion of the sample plate in a vertical direction with fast horizontal raster scans of the laser beam performed with a single-axis optical scanner allowed one to attain the acquisition rate up to ~ 150 pixel/s. The performance of the developed instrumentation was optimized using sprayed and sublimated model samples. Finally, the instrument was used to analyze 3D colorectal adenocarcinoma cell aggregates. Limitations of the technique throughput including the cleaning of the ion source are also discussed.

Experimental

Chemicals

Synthetic peptide, adrenocorticotrophic hormone fragment 18–39 (ACTH), 2,5-dihydroxybenzoic acid (DHB), trifluoroacetic

acid (TFA), and ethanol were purchased from Sigma-Aldrich (St. Louis, MO, USA). Methanol was purchased from Scharlau Chemie S.A. (Barcelona, Spain). All these chemicals were analytical-reagent grade.

Chemicals for the cell cultivation and spheroid treatment included high-glucose Dulbecco's modified Eagle's medium with sodium pyruvate (DMEM), fetal calf serum (FCS), MEM non-essential amino acids (100×), 2-mercaptoethanol (1.11 g/mL), phosphate-buffered saline (1× PBS) consisting of 8 g NaCl, 0.2 g KCl, 1.44 g Na₂HPO₄, 0.24 g KH₂PO₄ in a volume of 1,000 mL H₂O, pH 7.4, all from Sigma-Aldrich, and L-glutamine (200 mM in 0.85% NaCl solution), potassium penicillin (10,000 U/mL), and streptomycin sulfate (10,000 µg/mL), all from Lonza, Verviers, Belgium. An antitumor agent perifosine for drug assay was obtained from Cayman Chemical Company (Ann Arbor, MI, USA). Gelatin powder Castello (Lidl Stiftung & Co. KG, Neckarsulm, Germany) was purchased in a local drug store.

Preparation of Model Samples

To prepare samples for MSI, both airbrush spraying and sublimation were employed.

Airbrush

Forty milligrams of DHB matrix was dissolved in 1 mL of 80:20 (v/v) methanol/water solution containing 0.2% TFA. The matrix solution was mixed with 20 µM ACTH aqueous solution in the ratio 1:1 (v/v). The 200 µL of the mixture was continuously sprayed on a stainless steel MALDI plate using an airbrush pistol GRAFO T1 (Harder & Steenbeck Airbrush, Norderstedt, Germany) with a 0.15 mm orifice from a distance of 8 cm under a working pressure of 300 kPa.

Sublimation

To prepare a homogenous layer of matrix suitable for optimization of instrumental parameters, DHB was sublimated onto the stainless steel MALDI target in a glass sublimation apparatus GPE-1207-030PS (GPE Scientific Ltd., Bedfordshire, United Kingdom) embedded in a heated aluminum block. Approximately 0.1 g of DHB was placed at the bottom of the apparatus and the sublimation to the MALDI target was carried out at 120 °C and 80 mTorr pressure for 5 min, resulting in 0.24 mg/cm² DHB coverage as determined from the weight difference.

Cell Culture and Tumor Spheroid Formation

Human colorectal adenocarcinoma HT-29 (ATCC®, HTB-38™) cells from LGC Standards, Teddington, UK, were cultivated in DMEM supplemented with 10% FCS, 2 mM L-glutamine, 100 U/mL penicillin, and 100 µg/mL streptomycin in humidified 5% CO₂ atmosphere at 37 °C.

Human foreskin fibroblasts (ATCC®, SCRC 1041™) from LGC Standards were cultivated in DMEM supplemented with 15% FBS, 2 mM L-glutamine, 100 U/mL penicillin, and

100 µg/mL streptomycin, non-essential amino acids, and 0.01 mM beta-mercaptoethanol.

For multicellular spheroid formation, the HT-29 cells were washed with 1 mM EDTA in 1× PBS, mixed with fibroblasts (1:1) and seeded at a density of 50,000 cells/mL on the 12-well plate in DMEM supplemented with 1% FBS and 2 mM L-glutamine. The cellular mixture was incubated on a rotary shaker (60 rpm, Orbital Shaker, NB-101SRC, N-BIOTEK, Korea) in humidified 5% CO₂ atmosphere at 37 °C for 1 day. Then, the culture medium was removed and replaced with fresh DMEM medium supplemented with 10% FBS, 2 mM L-glutamine and the spheroids were cultivated for 5 days. The grown spheroids were treated with 20 µM perifosine for 24 h.

Preparation of Spheroids for MALDI MSI

After drug treatment, the cultivation medium was removed and the spheroids were washed three times with 1× PBS. Half a milliliter of warm 180-mg/mL gelatin solution in water was placed in particular wells of a 24-well plate and spheroids were transferred into gelatin using a pipette with a truncated tip. Spheroids were overlaid with another 500 µL of the gelatin solution and left at room temperature until solidification was completed. Samples were then frozen at -80 °C and stored until analysis.

The spheroids in gelatin were freeze-sectioned (-27 °C) into 12-µm-thick slices using cryostat CM1850 (Leica, Heidelberg, Germany). The slices were thaw-mounted onto stainless steel MALDI plates. The plates were then placed in a desiccator prior to the matrix deposition. DHB matrix was sublimated onto the plates in the sublimation apparatus according to the procedure described above. The samples were dried in a desiccator for 30 min before analysis.

The spheroid slices were visually inspected before and after the MSI analysis using a stereo microscope, model STM 823 (INTRACO MICRO, Tachlovice, Czech Republic) equipped with a digital camera, model Nikon D5100 (Nikon Corporation, Tokyo, Japan).

Laboratory-Built Mass Spectrometer

A laboratory-built axial MALDI TOF mass spectrometer used for high-throughput MSI was equipped with a galvanometer-based optical scanner (6810P; Cambridge Technology, Lexington, MA) inserted into the optical pathway of the UV laser. The reflector TOF MS instrument with a 2.6-m-long drift tube was operated in the positive mode with the delayed pulse ion extraction. Since our previous work [30], important upgrades to the instrument were made. First, a diode-pumped frequency-tripled 355 nm Nd:YAG laser FTSS355-Q2-OEM (CryLaS GmbH, Berlin, Germany) operated at repetition rates of up to 5 kHz with maximal output energy 6.6 µJ per pulse was installed. The laser pulse energy was measured directly inside the MALDI source by the Laser Thermal Power Sensor 3A-P-SH-V1-ROHS (Ophir Photonics, North Logan, UT, USA). Second, to maintain a stable voltage output of the DC and pulsed power supplies of our mass spectrometer at 5-kHz

pulsing rate, the delayed pulse extraction circuitry was rebuilt using a push-pull high voltage pulser (Behlke, Germany). Third, the original ion mirror taken from an ABI 4700 TOF/TOF MS instrument was made longer by a factor of two. The use of longer mirror led to a reduction in the ion scattering caused by the field inhomogeneity near the mirror grids, which resulted in a significant improvement in mass resolving power [32].

For a detailed description of the mass spectrometer with pulse extraction circuitry and dual-stage ion mirror, see the Supplementary material. The modification of the ion source is discussed in the “Results and Discussion” section below.

In the absence of a laser pulse, the DC voltage applied to both the ion repeller and extraction electrode was kept at a level of 10.50 kV. A 4.70-kV 10- μ s-long pulse delayed by 475 ns, with respect to the laser pulse, was applied across the gap between the repeller and the extraction grid to perform the ion extraction. The voltages applied across the first and second stages of the ion mirror were 10.98 kV and 15.80 kV, respectively. Using these settings for measurement of ACTH fragment 18–39 with mass 2,465 Da, a resolving power of up to 25,000 was attained.

The instrument was controlled by a software program developed in the LabVIEW programming environment (*Spectrometer Control*). The software program controlled the travel of X and Y stages, the angular position of the mirror in the optical scanner, as well as signal acquisition, data processing, and data storage in imzML format. The MSI experiments were carried out using either the flyback or meandering scan patterns, horizontal linescan scan type, left-right linescan direction (first linescan), and bottom-up linescan sequence. Note that these scanning mode descriptors are given in accordance with the imzML terminology [33].

Results and Discussion

Design of the Ion Source

The ion source comprises a MALDI target, serving also as the repeller electrode, the ion extraction, and acceleration grid electrodes both with 508- μ m mesh size. The individual wires of the electrodes are 33.0–40.6 μ m thick, as stated by the manufacturer (Jordan TOF Products, Inc., Grass Valley, CA, USA). Details and dimensions of the ion source are given in Figure 1a.

In our previous work [30], we proved the concept of fast MSI using rapid laser beam microscans. Originally, the laser beam was focused onto the sample surface by a lens with a 254-mm focal length at an angle of 20° (referenced to the axis orthogonal to the plate) bypassing both grid electrodes to prevent the laser beam from being blocked by the grids. However, this resulted in the elliptic shape of the laser spot on the MALDI target, which limited the MSI lateral resolution along the horizontal axis. Obviously, a much better lateral resolution can be achieved by decreasing the angle of incidence and aiming the laser beam through the grids, thus producing a

circular spot. To further decrease the spot size, a lens with a shorter focal length should be used.

Based on these premises, the angle of incidence of the laser beam was decreased to 20°. In this arrangement, the laser beam passed through both grid electrodes of the ion source as shown in Figure 1a. To get unobstructed laser beam scans in the horizontal direction, two short sections of vertical wires of the ion extraction electrode grid were excised using UP-266 Macro Laser Ablation System (New Wave Research, Inc., Fremont, CA, USA) with the size of the ablation laser spot 100 μ m, laser fluence \sim 15 J/cm², and frequency 10 Hz. A rectangular window 1.5 \times 0.5 mm was formed in the ion extraction grid. The grid covering the acceleration electrode was left unmodified. The laser beam was expanded using a beam expander to reduce the percentage of the beam blocked by the wires of this electrode. To reduce the laser spot size, the original focusing lens with the focal length 254 mm was replaced with a 76-mm focal length lens positioned inside the ion source. This was the shortest focal length allowed by the geometry of the ion source. The scanning mirror was located outside the vacuum chamber, 150 mm from the focusing lens. In the given arrangement, a single wire of the grid covering the ion acceleration electrode blocked only 7–11% of the laser beam the cross section of which was determined by the diameter of the iris aperture being set to 3–2 mm, respectively. The opening of the iris aperture also determined the laser spot size on the target plate. In the same arrangement, had the pair of wires in the grid of the ion extraction electrode not been removed, it would have blocked up to 26–38% of the laser beam.

Spot Size

The modification of the UV laser optics and reduction of the angle of incidence to 20° allowed the formation of a nearly circular laser spot with a top-hat intensity distribution on the MALDI target. The laser spot size was determined by microscopic inspection of the burnt spots in a sublimated layer of the DHB matrix. The spots were burnt using 50- μ m steps in the laser beam scanning mode. Approximately 20 laser pulses were sufficient to completely ablate a thin layer of DHB. The laser pulse energy was adjusted by the variable density filter in the range of 0.09 to 0.20 μ J. Spots with a diameter of 10–20 μ m were obtained (see Figure 2), which provided lateral resolution and sensitivity adequate for most MSI applications.

Scan Range

The distance the UV laser beam can travel along the sample surface is restricted by the 1.5-mm-long rectangular window made in the mesh grid covering the extraction electrode. The practical range of the laser scan was expected to be narrower than 1.5 mm to avoid any part of the laser beam impinging the grid wires. The practical scan range was experimentally determined by performing the laser beam scan producing a 2-mm-long horizontal trace burnt in a homogenous sublimated layer of DHB. Regions 2.0 \times 0.2 mm on the target were irradiated using 20- μ m raster (100 \times 10 pixels, 20 pulses per pixel,

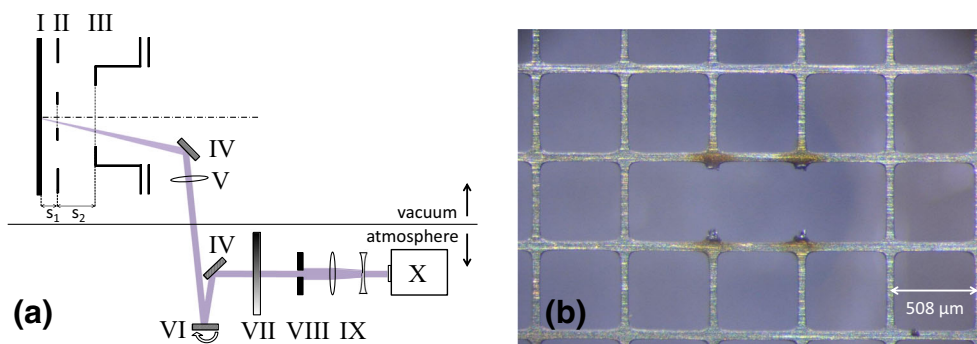


Figure 1. The ion source. (a) MALDI source schematic diagram (the distances are not in scale). (I) MALDI target (repeller); (II) ion extraction electrode, $s_1 = 4.5$ mm; (III) ion acceleration electrode, $s_2 = 12.5$ mm; (IV) mirrors; (V) focusing lens (focal length = 76 mm); (VI) scanning mirror; (VII) variable density filter; (VIII) iris aperture; (IX) 3.5 \times beam expander; (X) UV laser. (b) Image of the grid covering the ion extraction plate modified to achieve the horizontal laser beam microscans

0.14 $\mu\text{J}/\text{pulse}$). The recorded signal of $[2\text{DHB}-2\text{H}_2\text{O}+\text{H}]^+$ ions ($m/z = 273.0 \pm 0.1$) from each of the 100 columns was averaged and plotted vs. the x -axis position. As expected, two minima due to blocking of the laser beam by the wires at the borders of the 1.5-mm window were observed in the resulting plot, see Figure 3a. The width of the plateau between minima defined the maximum beam scan range of 1.2 mm.

Comparison of the Scanning and the Translation Modes

To explore the signal intensity and mass resolving power in the scanning mode compared to the translation mode, a sublimated DHB layer and then a sprayed layer of DHB containing ACTH were used. To assess the impact of laser energy on the quality of MS images, the 2×0.2 -mm rectangular areas (strips) of sublimated DHB layer were imaged with a 20- μm spacing between the pixels (100×10 pixels, 20 shots per pixel) using 2-mm-long laser scan. Signal intensity profiles of $[2\text{DHB}-2\text{H}_2\text{O}+\text{H}]^+$ ion at $m/z 273.0 \pm 0.1$ were recorded using the laser pulse energies varied from 0.05 to 0.28 μJ set up by the variable density filter and iris aperture. Again, the signals from pixels with the same x -axis coordinate were averaged and plotted vs. the x -axis coordinate. Working near the MALDI signal threshold utilizing reduced laser energy or diminishing beam diameter using the iris diaphragm (thus achieving < 10 μm spot size),

two local minima in the scanned signal intensity profile were observed (Figure 3b, c) in addition to two border minima caused by the ion extraction electrode grid wires at the borders of the window. These local minima were the result of the laser beam hitting the vertical wires of the ion acceleration grid and were found to strongly depend on the laser pulse energy. At a laser pulse energy 0.09 μJ and higher, the local minima vanished leaving signal plateau within the window suitable for MSI.

In another experiment, the sprayed sample with DHB matrix containing 10 μM ACTH has been used. The signal of the protonated ACTH at $m/z 2,465.2 \pm 0.1$ was monitored at different laser energies. The 2.0×0.4 -mm strips were imaged with 20- μm raster spacing (100×20 pixels, 50 shots per pixel). In accordance with the experiments with the sublimated DHB layer, the periodical ACTH signal changes in signal profile along x -axis vanished at laser energies 0.09 μJ and higher, see Figure 3d–f. Using the scan mode, values for relative standard deviations (*RSD*) of the ACTH signal intensity were calculated from areas that accommodated 1,200 (i.e., 60×20) pixels representing the signal plateau. The values were averaged over three different areas selected within the same MALDI plate and compared to those obtained from similar sample areas on the same plate using the translation mode (the laser beam is fixed but the plate moves). *RSD* values recorded at 0.09 μJ were $37\% \pm 3\%$ and $37\% \pm 5\%$ for scanning and translation mode,

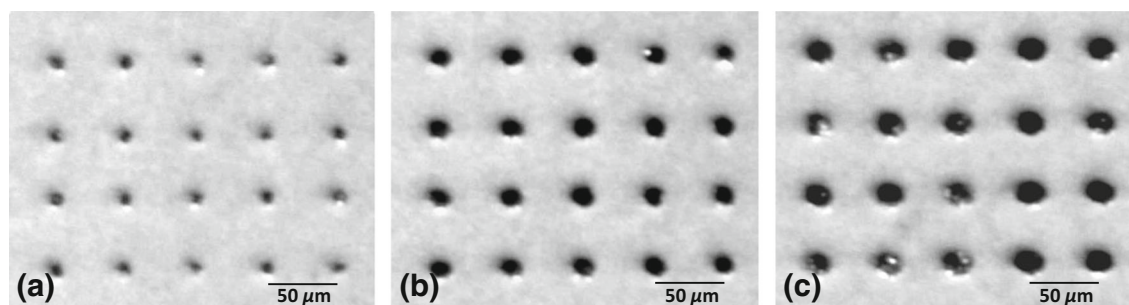


Figure 2. Spots burnt in a sublimated layer of DHB by 20 shots at laser pulse energies (a) 0.09 μJ (measured spot size in horizontal and vertical dimensions was 9.9 ± 0.7 and 9.4 ± 0.8 μm , correspondingly), (b) 0.14 μJ (15.8 ± 1.0 and 14.5 ± 1.0 μm), and (c) 0.20 μJ (21.7 ± 1.9 and 18.9 ± 0.9 μm). Small bright spots occasionally appearing in the burnt areas are the light reflection from imperfections on the metal target

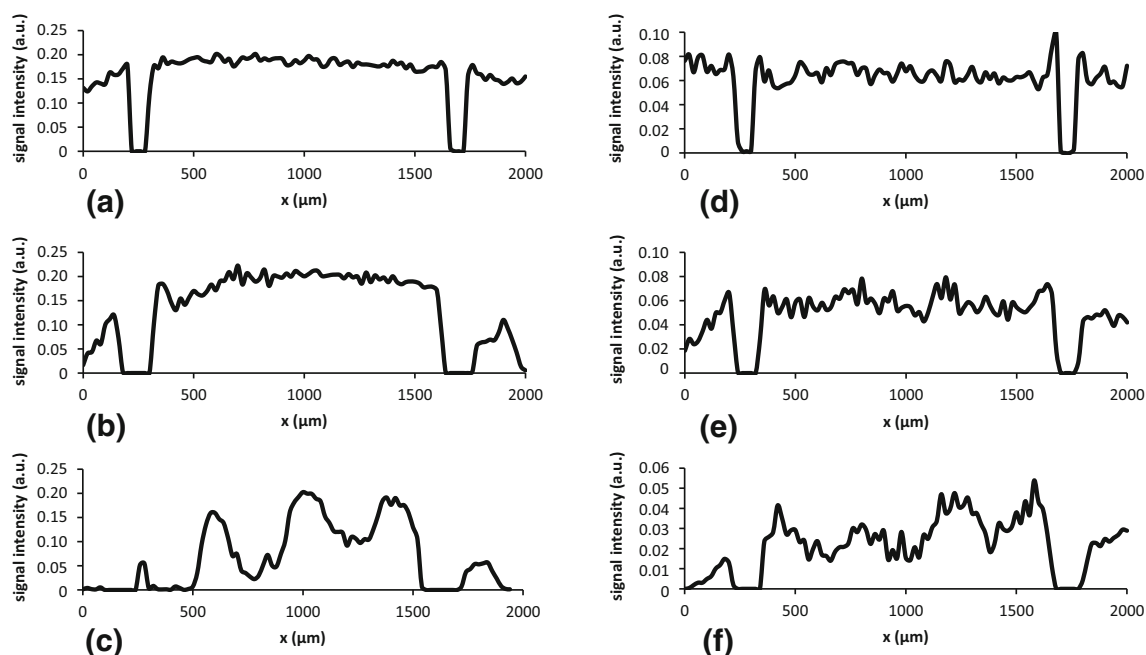


Figure 3. Signal intensity profiles of $[2\text{DHB}-2\text{H}_2\text{O}+\text{H}]^+$ ion peak, $m/z = 273.0 \pm 0.1$ averaged over 2-mm-long laser beam scans, each being recorded using step $20 \mu\text{m}$ from the sublimated layer of DHB at laser energy (a) $0.14 \mu\text{J}/\text{pulse}$; (b) $0.09 \mu\text{J}/\text{pulse}$; (c) $0.07 \mu\text{J}/\text{pulse}$ and signal intensity profiles of $[\text{ACTH}+\text{H}]^+$, $m/z = 2465.2 \pm 0.1$ recorded from the sprayed DHB sample at laser energy (d) $0.14 \mu\text{J}/\text{pulse}$; (e) $0.09 \mu\text{J}/\text{pulse}$; and (f) $0.07 \mu\text{J}/\text{pulse}$

respectively. Similar *RSD* values were obtained for higher laser energies. The large variation in *RSD* observed in the both modes most likely reflects a general inhomogeneity of the sprayed DHB sample. The mass resolving power at $m/z = 2,465.2$ was stable at approximately 25,000 over the entire plateau region. In summary, scanning the laser beam along 1-mm-long stretches in the modified source did not lead to any observable deterioration in either signal level or mass resolving power compared to the translation mode with a fixed laser beam.

Scan Pattern

The laser beam is usually moved across the sample in the MSI experiment in one of two different scan patterns: flyback or meandering. In the flyback or sometimes called typewriter scan pattern, MS data are acquired by performing linescans only in one direction, while the meandering or serpentine scan pattern indicates that the linescans are executed in alternating directions. The meandering scan pattern is naturally faster using translation-based sampling mode, as it does not require movement of the sample back to the starting point following completion of each linescan. On the contrary, the laser beam scanning mode is not limited by target translation and the laser can be redirected back to the starting point almost instantly using the optical scanner. Thus, the flyback and meandering scan patterns are equal in speed when using the laser beam scanning mode on MSI of areas with a smaller or equal width than that of the scan range.

The intensity of mass peaks obtained in flyback and meandering scan patterns were compared by scanning the

sublimated DHB matrix layer. In a low lateral resolution scan mode, i.e., where adjacent burnt $10\text{-}\mu\text{m}$ spots did not overlap, data looked similar for the both scan patterns. In the high lateral resolution experiments where adjacent spots slightly overlapped or were burnt in very close proximity to each other, the meandering scan pattern yielded different ion intensities dependent on the direction of the laser beam motion. This led to alternating horizontal strips with high and low intensities in the MS images (see Figure S5 in the Supplementary material). There are several possible explanations for this phenomenon. Signal intensity can be affected by the deposits of the ablated matrix on adjacent pixels. In our case, the laser irradiated the sample at a 20° angle of incidence and more material was expected to be deposited on the side of the laser beam incidence. The second possible reason is inhomogeneity of the laser beam profile, which leads to the formation of differently shaped craters on the sample surface. The laser beam irradiation of a differently skewed region could change the ion plume direction, possibly affecting ion transmission and thus the signal intensity. The flyback scan pattern was found to provide stable ion intensities without any “directional” influence in all experiments and was used thereafter.

MALDI MSI Acquisition Rate

The reduction of the laser spot size down to $10 \mu\text{m}$ allowed taking spectra from 100 individual and well-defined pixels per a 1-mm-long linescan without any movement of the motorized stages, markedly increasing the MSI acquisition rate of the instrument. The performance of the combined stage translation

and laser beam scanning mode was evaluated using 10,000 pixel images with 10–100 μm raster (i.e., area $1 \times 1-10 \times 10$ mm) and 10–100 laser shots per pixel. To estimate the effect of the amount of data created and stored, the images were recorded with 40,000 or 100,000 data points per TOF spectrum (1-ns time bins, 32-bit stored data per bin), resulting in 1.6 or 3.9 GB imzML files, respectively. The total imaging time was recorded and used to calculate the acquisition rate.

The more pixels acquired in a single linescan with the laser beam, the higher the gain in acquisition rate is as less stage translations between the scan segments (lines) are required. This trend is illustrated in Figure 4, which shows an increase in the acquisition rate with the reduction of the pixel size.

Overall, the acquisition rate was limited by the slowest of the three repeating events: the spectrum acquisition, pixel-to-pixel translation, and data processing/storage. It has to be noted that certain time was also spent on software control and command sending. This time was not explicitly measured and it is included in the data processing/storage time.

Employing the traditional target translation mode at 5-kHz repetition rate, MS images were recorded with 6–10 pixel/s acquisition rates. The rate-limiting step was the pixel-to-pixel translation, the size and duration of which were defined by the pixel size. Reduction of the number of laser shots fired per pixel from 100 to 10 and the decrease of stored data points per spectrum from 100,000 to 40,000 had a minor effect on the acquisition rate, which increased only by 0.5 pixel/s and 1.5 pixel/s, respectively.

The MSI acquisition rate in the laser beam scanning mode was determined by all three parameters, dependent on the particular measurement conditions. Using 100 μm pixels, the

pixel-to-pixel translation was the rate-limiting factor with 30 ms per pixel, approximately. With the reduction of the pixel size to 10 μm , the pixel-to-pixel translation time shortened to approximately 2 ms due to dominant involvement of the optical scanner in pixel addressing. Also, when using 100 laser shots per pixel, the acquisition rate was limited to 40 pixel/s by spectra acquisition (20 ms per pixel at 5 kHz). Going down to 10 shots per pixel, the acquisition rate further rose to values over 100 pixel/s and the data processing/storage became a major consideration with approximately 6 ms per pixel. Finally, storing 40,000 instead of 100,000 data points per pixel increased the acquisition rate to 147 pixel/s. Still, the data processing/storage rate was the major limiting factor, adding approximately 3 ms per pixel. This time constraint is expected to gradually diminish due to the constantly increasing speed of processors.

In another experiment, an area of 10×10 mm was imaged with 10 laser shots per pixel and 40,000 data points per TOF spectrum in the combined stage translation and laser beam scanning mode. The pixel size was set to 10, 20, or 50 μm , yielding 1, 0.25, or 0.04 Mpixel images which were acquired in 2.95, 1.04, or 0.32 h with acquisition rates 94, 67, and 35 pixel/s, respectively. In the case of 10, 20, or 50 μm pixels, the scanning mirror is repositioned 100, 50, or 20 times per a single X stage step. The more movements the scanning mirror makes at a given X stage position, the faster acquisition rate is.

In summary, utilizing the 5-kHz laser and 1-mm-long laser beam scans provided an acquisition rate of 147 pixel/s for 10- μm raster with 10 pulses fired per pixel and 40,000 data points in the spectra, see Figure 4. This performance surpasses the maximal published acquisition rate 50 pixel/s of the above

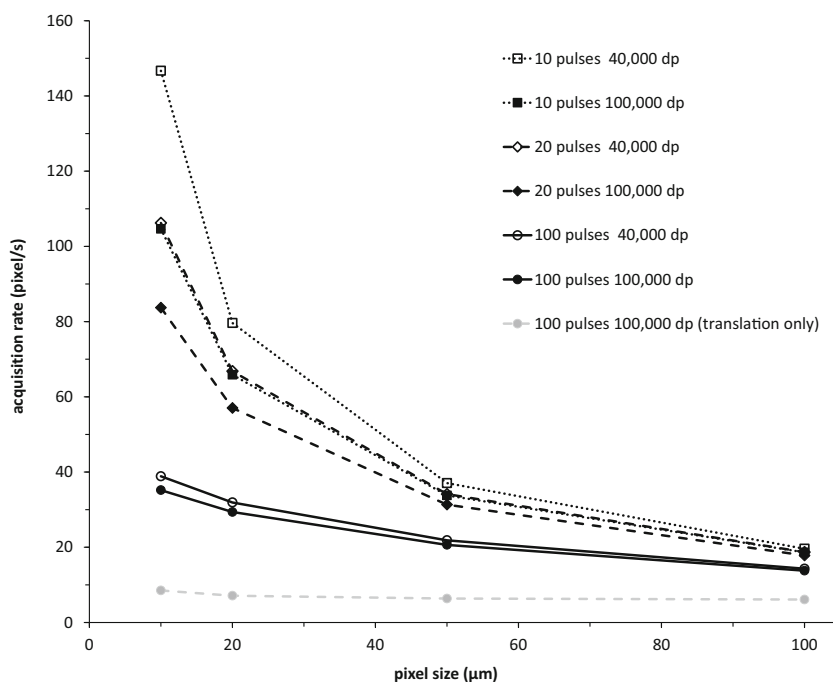


Figure 4. MSI acquisition rate in laser beam scanning and target translation mode utilizing flyback scan pattern as a function of the pixel size, number of laser shots per pixel (pulses), and data points per spectrum (dp). Laser repetition rate was 5 kHz

mentioned commercial MALDI TOF MS instrument with two optical scanners [11]. MSI acquisition rates of 100 pixel/s were so far reported only for inductively coupled plasma (ICP) TOF MS system for elemental mapping of the surfaces [34].

Imaging of 3D Cell Aggregates

3D cell cultures commonly known as spheroids are aggregates of cells (not always necessarily with a fully symmetrical shape) [35] analogous to tissue as established by Sutherland et al [36–38]. In vitro models based on the 3D cell cultures offer a high degree of clinical significance and represent a reasonable compromise between traditional monolayer cultures and in vivo tumors. As such, spheroids are often used as realistic in vitro models for the systematic study of the tumor response to a therapy. In the recent years, the number of MS imaging studies on spheroids is constantly growing [39–42].

To illustrate a remarkably high MS image acquisition rate using laser beam scans, sections of perifosine-treated spheroids embedded in gelatin were imaged. The 1.0×1.3 mm and $2.0 \times$

2.0 mm MS images with spatial resolution of $10 \mu\text{m}$, 10 laser pulses ($0.09 \mu\text{J}/\text{pulse}$) fired at each pixel, averaged spectrum from each pixel comprising 60,000 data points (1-ns time bins containing 32-bit intensity values) were recorded at acquisition rates of 130 and 100 pixel/s, respectively. Only mirror was employed for horizontal scanning to acquire the smaller image, while the X stage had to move 1 mm within each horizontal scan to stitch two segments scanned by the optical scanner in the case of the larger image. Figure 5 shows optical and MS images of two spheroids with 0.8 mm diameter (top panel) and 1.0 mm (bottom panel). The optical images (Figure 5a, e) were taken prior DHB application. Perifosine was detected in both spheroid samples; its distribution can be seen in Figure 5c, g. Comparison of MALDI MS and optical images reveals that perifosine is located just in the outer boundary of spheroids with a penetration depth of approximately $100 \mu\text{m}$. In addition, perifosine was observed outside spheroids. Most likely, it diffused out from spheroid cells during gelatine embedment. For comparison, distribution of cholesterol fragment ion $[M-\text{H}_2\text{O}+\text{H}]^+$ is shown in Figure 5b, f and distribution of

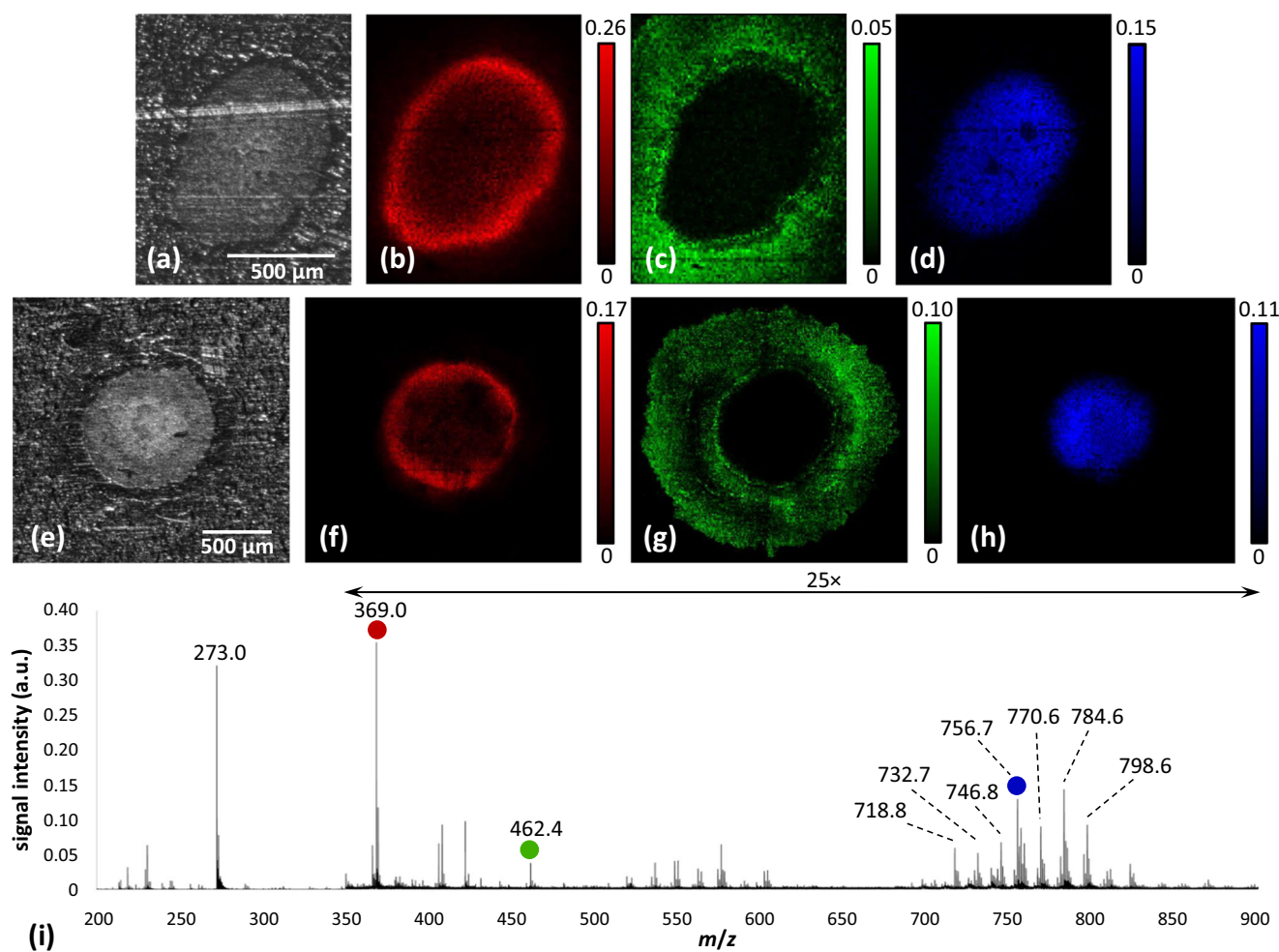


Figure 5. Images of two spheroids with diameters 0.8 and 1.0 mm. (a, e) Photographs and MS images of (b, f) cholesterol fragment $[M-\text{H}_2\text{O}+\text{H}]^+$, (c, g) perifosine, and (d, h) $[\text{PC}(32:0)+\text{Na}]^+$ distributions at $m/z = 369.0 \pm 0.1$, 462.4 ± 0.1 , and 756.7 ± 0.1 , respectively. (i) Average mass spectrum of the spheroid in (a). The values of arbitrary units on scale bars represent integrated signal intensity over the selected m/z range

phosphatidylcholine [PC(32:0)+Na]⁺ in Figure 5d, h. The signal-to-noise ratios for the imaged analytes were comparable (within a factor of 2) to those obtained with a commercial TOF mass spectrometer (Autoflex speed, Bruker) recorded under almost similar conditions. For more information about sensitivity evaluation, see the Supplementary material.

Conclusions

In this work, we presented a high-speed high-resolution MALDI TOF MS system with a novel design of the ion source capable of providing raster imaging with a pixel size down to 10 μm. An optical scanner capable of redirecting the laser beam in less than 300 μs was employed to perform 1-mm laser beam horizontal linescans across the sample at fixed position of MALDI plate. In the end of linescan, the sample plate was moved in a vertical direction using the motorized stage. A small rectangular window created in the grid electrode used for ion extraction allowed unimpeded redirecting of the laser beam along the sample under a small incident angle while providing a nearly circular laser spot. As the optical scanner moved the laser spot in precisely controlled steps, images were recorded from discrete pixels with the size limited by the minimum laser spot size. A 10-μm pixel size represents a practical limit for many imaging applications, as the MALDI ions significantly drop with further decreasing of the laser spot diameter [43]. It is worth to note that the lateral resolution at a level of 1–3 μm could not be easily achieved by using sublimation matrix deposition chambers or commercial automated matrix spraying systems due to the formation of microcrystals. So in many instances, going below 10-μm resolution can be impeded due to a practical limit established by matrix deposition methods as well as rapid reduction in the ion yield. The employed 5-kHz laser repetition rate provides a reasonable mass range for axial TOF systems, as the upper *m/z* is limited by the time (200 μs) between laser shots. In our system, the upper mass limit was about 7,000 Da at 15 kV acceleration voltage, which is adequate for most frequently imaged molecules. MSI of larger molecules would be possible in linear mode with upper mass limit around 20,000 Da for the same instrument. Applying higher acceleration voltages, e.g., 30 kV, while other conditions are the same will lead to approximately 40% increase in either the upper mass limit or acquisition speed as well as improve mass resolution due to the reduction in the turn-around time [44].

The long-term stability of the modified TOF MALDI mass spectrometer was found to be quite remarkable: its operation was found to be resistant to the contamination of the grids by ablated matrix/tissue debris and the ion source was easy to clean. Firing 40 million laser shots at rather high pulse energy did not result in deterioration of the MS instrument performance in terms of sensitivity, mass accuracy, or mass resolving power; see the Supplementary material for details.

The developed MSI technique is most advantageous for acquisition of high-resolution images (utilizing 10-μm laser

spots) from relatively small (about 1–2 mm wide) sample area which dimensions are comparable to the length of horizontal optical scan. The developed high-throughput instrument was utilized to map a distribution of perifosine in 3D colorectal adenocarcinoma cell aggregates with high spatial resolution. The achieved acquisition rate of approximately 150 pixel/s was comparable to or surpassed that demonstrated by recently introduced commercial instruments [12, 31]. Still, the efficient sample acquisition rate demonstrated in this study was 3-fold lower than the one calculated from the total axial re-TOF MS instrument time. A theoretical limit of 500 pixel/s (10 laser pulses per pixel at 5-kHz laser repetition rate, 200 μs between individual mass spectra) was not achieved mainly due to limitation in the speed with which both software and hardware record and store the data. Anticipated improvements in the performance of both data acquisition hardware and data processing software as well as optimization of the program code will lead to a substantial increase in MSI throughput.

Acknowledgments

We gratefully acknowledge the financial support of the Grant Agency of the Masaryk University (MUNI/G/0974/2016), the Czech Science Foundation (GA 15-05387S) and the Ministry of Education, Youth and Sports of the Czech Republic under the projects CEITEC 2020 (LQ1601), Translational Medicine (LQ1605) and NETME CENTRE PLUS (LO1202).

References

1. Yang, J.H., Caprioli, R.M.: Matrix pre-coated targets for high throughput MALDI imaging of proteins. *J. Mass Spectrom.* **49**, 417–422 (2014)
2. Stoeckli, M., Staab, D.: Reproducible matrix deposition for MALDI MSI based on open-source software and hardware. *J. Am. Soc. Mass Spectrom.* **26**, 911–914 (2015)
3. Hankin, J.A., Barkley, R.M., Murphy, R.C.: Sublimation as a method of matrix application for mass spectrometric imaging. *J. Am. Soc. Mass Spectrom.* **18**, 1646–1652 (2007)
4. Thomas, A., Charbonneau, J.L., Fournais, E., Chaurand, P.: Sublimation of new matrix candidates for high spatial resolution imaging mass spectrometry of lipids: enhanced information in both positive and negative polarities after 1,5-Diaminonaphthalene deposition. *Anal. Chem.* **84**, 2048–2054 (2012)
5. Schuereberg, M., Luebbert, C., Deininger, S.O., Ketterlinus, R., Suckau, D.: MALDI tissue imaging: mass spectrometric localization of biomarkers in tissue slices. *Nat. Methods.* **4**, iii–iv (2007)
6. Bouschen, W., Schulz, O., Eikel, D., Spengler, B.: Matrix vapor deposition/recrystallization and dedicated spray preparation for high-resolution scanning microprobe matrix-assisted laser desorption/ionization imaging mass spectrometry (SMALDI-MS) of tissue and single cells. *Rapid Commun. Mass Spectrom.* **24**, 355–364 (2010)
7. Rompp, A., Spengler, B.: Mass spectrometry imaging with high resolution in mass and space. *Histochem. Cell Biol.* **139**, 759–783 (2013)
8. Kompauer, M., Heiles, S., Spengler, B.: Atmospheric pressure MALDI mass spectrometry imaging of tissues and cells at 1.4-μm lateral resolution. *Nat. Methods.* **14**, 90–96 (2017)
9. Spraggins, J.M., Caprioli, R.: High-speed MALDI-TOF imaging mass spectrometry: rapid ion image acquisition and considerations for next generation instrumentation. *J. Am. Soc. Mass Spectrom.* **22**, 1022–1031 (2011)
10. Andersson, M., Groseclose, M.R., Deutch, A.Y., Caprioli, R.M.: Imaging mass spectrometry of proteins and peptides: 3D volume reconstruction. *Nat. Methods.* **5**, 101–108 (2008)

11. Prentice, B.M., Chumbley, C.W., Caprioli, R.M.: High-speed MALDI MS/MS imaging mass spectrometry using continuous raster sampling. *J. Mass Spectrom.* **50**, 703–710 (2015)
12. Potocnik, N.O., Porta, T., Becker, M., Heeren, R.M.A., Ellis, S.R.: Use of advantageous, volatile matrices enabled by next-generation high-speed matrix-assisted laser desorption/ionization time-of-flight imaging employing a scanning laser beam. *Rapid Commun. Mass Spectrom.* **29**, 2195–2203 (2015)
13. Cornett, D.S., Frappier, S.L., Caprioli, R.M.: MALDI-FTICR imaging mass spectrometry of drugs and metabolites in tissue. *Anal. Chem.* **80**, 5648–5653 (2008)
14. Schober, Y., Guenther, S., Spengler, B., Rompp, A.: High-resolution matrix-assisted laser desorption/ionization imaging of tryptic peptides from tissue. *Rapid Commun. Mass Spectrom.* **26**, 1141–1146 (2012)
15. Belov, M.E., Ellis, S.R., Dillillo, M., Paine, M.R.L., Danielson, W.F., Anderson, G.A., de Graaf, E.L., Eijkel, G.B., Heeren, R.M.A., McDonnell, L.A.: Design and performance of a novel Interface for combined matrix-assisted laser desorption ionization at elevated pressure and electrospray ionization with Orbitrap mass spectrometry. *Anal. Chem.* **89**, 7493–7501 (2017)
16. Moskovets, E., Misharin, A., Laiko, V., Doroshenko, V.: A comparative study on the analytical utility of atmospheric and low-pressure MALDI sources for the mass spectrometric characterization of peptides. *Methods.* **104**, 21–32 (2016)
17. Soltwisch, J., Ketting, H., Vens-Cappell, S., Wiegelmann, M., Muthing, J., Dreisewerd, K.: Mass spectrometry imaging with laser-induced postionization. *Science.* **348**, 211–215 (2015)
18. Ellis, S.R., Soltwisch, J., Paine, M.R.L., Dreisewerd, K., Heeren, R.M.A.: Laser post-ionisation combined with a high resolving power orbitrap mass spectrometer for enhanced MALDI-MS imaging of lipids. *Chem. Commun.* **53**, 7246–7249 (2017)
19. Schwartz, M., Meyer, B., Wimitzer, B., Hopf, C.: Standardized processing of MALDI imaging raw data for enhancement of weak analyte signals in mouse models of gastric cancer and Alzheimer's disease. *Anal. Bioanal. Chem.* **407**, 2255–2264 (2015)
20. Schramm, T., Hester, A., Klinkert, I., Both, J.P., Heeren, R.M.A., Brunelle, A., Laprevote, O., Desbenoit, N., Robbe, M.F., Stoeckli, M., Spengler, B., Rompp, A.: imzML - a common data format for the flexible exchange and processing of mass spectrometry imaging data. *J. Proteome.* **75**, 5106–5110 (2012)
21. Robbe, M.F., Both, J.P., Pridaux, B., Klinkert, I., Picaud, V., Schramm, T., Hester, A., Guevara, V., Stoeckli, M., Roempp, A., Heeren, R.M.A., Spengler, B., Gal, O., Haan, S.: Software tools of the Computis European project to process mass spectrometry images. *Eur. J. Mass Spectrom.* **20**, 351–360 (2014)
22. Caprioli, R.M.: Imaging mass spectrometry: enabling a new age of discovery in biology and medicine through molecular microscopy. *J. Am. Soc. Mass Spectrom.* **26**, 850–852 (2015)
23. Preisler, J., Hu, P., Rejtar, T., Moskovets, E., Karger, B.L.: Capillary array electrophoresis-MALDI mass spectrometry using a vacuum deposition interface. *Anal. Chem.* **74**, 17–25 (2002)
24. Moskovets, E., Preisler, J., Chen, H.S., Rejtar, T., Andreev, V., Karger, B.L.: High-throughput axial MALDI-TOF MS using a 2-kHz repetition rate laser. *Anal. Chem.* **78**, 912–919 (2006)
25. Jungmann, J.H., Smith, D.F., MacAleese, L., Klinkert, I., Visser, J., Heeren, R.M.A.: Biological tissue imaging with a position and time sensitive pixelated detector. *J. Am. Soc. Mass Spectrom.* **23**, 1679–1688 (2012)
26. Soltwisch, J., Goritz, G., Jungmann, J.H., Kiss, A., Smith, D.F., Ellis, S.R., Heeren, R.M.A.: MALDI mass spectrometry imaging in microscope mode with infrared lasers: bypassing the diffraction limits. *Anal. Chem.* **86**, 321–325 (2014)
27. Halford, E., Winter, B., Mills, M.D., Thompson, S.P., Parr, V., John, J.J., Nomerotski, A., Vallance, C., Turchetta, R., Brouard, M.: Modifications to a commercially available linear mass spectrometer for mass-resolved microscopy with the pixel imaging mass spectrometry (PImMS) camera. *Rapid Commun. Mass Spectrom.* **28**, 1649–1657 (2014)
28. Hazama, H., Aoki, J., Nagao, H., Suzuki, R., Tashima, T., Fujii, K., Masuda, K., Awazu, K., Toyoda, M., Naito, Y.: Construction of a novel stigmatic MALDI imaging mass spectrometer. *Appl. Surf. Sci.* **255**, 1257–1263 (2008)
29. Bednařik, A., Preisler, J., Kuba, P., Ertl, L., Tomalová, I., Rážová, I., Moskovets, E.: High throughput MS imaging using a fast scanning mirror. Poster TP 430 in 60th ASMS Conference on Mass Spectrometry and Allied Topics, Vancouver, Canada (2012)
30. Bednařik, A., Kuba, P., Moskovets, E., Tomalova, I., Krasensky, P., Houska, P., Preisler, J.: Rapid matrix-assisted laser desorption/ionization time-of-flight mass spectrometry imaging with scanning desorption laser beam. *Anal. Chem.* **86**, 982–986 (2014)
31. Spraggins, J.M., Rizzo, D.G., Moore, J.L., Noto, M.J., Skaar, E.P., Caprioli, R.M.: Next-generation technologies for spatial proteomics: integrating ultra-high speed MALDI-TOF and high mass resolution MALDI FTICR imaging mass spectrometry for protein analysis. *Proteomics.* **16**, 1678–1689 (2016)
32. Moskovets, E.V.: Optimization of the reflecting system parameters in the mass-reflector. *Appl. Phys. B Lasers Opt.* **53**, 253–259 (1991)
33. Imaging MS controlled vocabulary. <https://ms-imaging.org/wp/imzml/controlled-vocabulary/>. (Visited July 2018)
34. Straus, R.N., Carew, A., Sandkuijl, D., Closson, T., Baranov, V.I., Loboda, A.: Analytical figures of merit for a novel tissue imaging system. *J. Anal. At. Spectrom.* **32**, 1044–1051 (2017)
35. Fennema, E., Rivron, N., Rouwkema, J., van Blitterswijk, C., de Boer, J.: Spheroid culture as a tool for creating 3D complex tissues. *Trends Biotechnol.* **31**, 108–115 (2013)
36. Hamilton, G.: Multicellular spheroids as an in vitro tumor model. *Cancer Lett.* **131**, 29–34 (1998)
37. Sutherland, R.M.: Cell and environment interactions tumor model. *Science.* **240**, 177–184 (1988)
38. Sutherland, R.M., McCredie, J.A., Inch, W.R.: Growth of multicell spheroids in tissue culture as a model of nodular carcinomas. *J. Natl. Cancer Inst.* **46**, 113–120 (1971)
39. LaBonia, G.J., Lockwood, S.Y., Heller, A.A., Spence, D.M., Hummon, A.B.: Drug penetration and metabolism in 3D cell cultures treated in a 3D printed fluidic device: assessment of irinotecan via MALDI imaging mass spectrometry. *Proteomics.* **16**, 1814–1821 (2016)
40. Lukowski, J.K., Weaver, E.M., Hummon, A.B.: Analyzing liposomal drug delivery Systems in Three-Dimensional Cell Culture Models Using MALDI imaging mass spectrometry. *Anal. Chem.* **89**, 8453–8458 (2017)
41. Bakker, B., Eijkel, G.B., Heeren, R.M.A., Karperien, M., Post, J.N., Cillero-Pastor, B.: Oxygen-dependent lipid profiles of three-dimensional cultured human chondrocytes revealed by MALDI-MSI. *Anal. Chem.* **89**, 9438–9444 (2017)
42. Theiner, S., Van Malderen, S.J.M., Van Acker, T., Legin, A., Keppler, B.K., Vanhaecke, F., Koellensperger, G.: Fast high-resolution laser ablation-inductively coupled plasma mass spectrometry imaging of the distribution of platinum-based anticancer compounds in multicellular tumor spheroids. *Anal. Chem.* **89**, 12641–12645 (2017)
43. Feenstra, A.D., Duenas, M.E., Lee, Y.J.: Five Micron high resolution MALDI mass spectrometry imaging with simple, interchangeable, multi-resolution optical system. *J. Am. Soc. Mass Spectrom.* **28**, 434–442 (2017)
44. Wiley, W.C., McLaren, I.H.: Time-of-flight mass spectrometer with improved resolution. *Rev. Sci. Instrum.* **26**, 1150–1157 (1955)